

ATMOSPHERIC NEUTRINOS AT SUPER-KAMIOKANDE

KATE SCHOLBERG

Boston University, Dept. of Physics, 590 Commonwealth Ave.

Boston, MA 02215, USA

E-mail: schol@budoe.bu.edu

for

THE SUPER-KAMIOKANDE COLLABORATION

ABSTRACT

In 1998, the Super-Kamiokande announced evidence for the observation of neutrino oscillations based on measurements of the atmospheric neutrino flux¹⁾. This paper presents the updated results for fully and partially-contained events with 736 days of data, as well as upward-going muon results and a global analysis. Preliminary interpretations of the results in terms of various two-flavor oscillation hypotheses are presented.

1. Introduction

1.1. Atmospheric Neutrinos

Atmospheric neutrinos are produced by collisions of cosmic rays with atoms in the Earth's upper atmosphere. These collisions produce showers which include neutrinos with energies in the 0.1 GeV to 100 GeV range. Although calculations of the absolute flux of atmospheric neutrinos^{2,3)} have fairly large uncertainties ($\sim 20\%$), the ratio of muon to electron flavor content is much better known (to $\sim 5\%$), since it arises from the decay chain $\pi \rightarrow \mu\nu_\mu, \mu \rightarrow e\nu_\mu \nu_e$. The muon to electron flavor ratio is expected to be about 2 (one ν_e from muon decay for every two ν_μ), gradually rising at energies above about 5 GeV as the muons from π decay have enough energy to survive to the surface of the earth and range out before decaying.

Because the attenuation of even high energy neutrinos in the earth is so small, neutrinos produced all around the atmosphere can be detected. Their pathlengths range from about 15 km for neutrinos produced directly overhead, to 13000 km for neutrinos produced directly below. The pathlength of the neutrino can be inferred from the direction of the Cherenkov cone of its produced lepton. Therefore, by measuring the zenith angle, energy and flavor of atmospheric neutrinos, we can test the neutrino oscillation hypothesis, which gives the probability of flavor conversion:

$$P_{f \rightarrow g} = \sin^2 2\theta \sin \left(\frac{1.27 \Delta m^2 (\text{eV}^2) L (\text{km})}{E_\nu (\text{GeV})} \right). \quad (1)$$

1.2. The Super-Kamiokande Detector

The Super-Kamiokande (Super-K) experiment is a large water Cherenkov detector located in Mozumi, Japan. Its total mass of ultra-pure water is 50 kton, divided into two concentric cylinders: an inner volume with its inside surface covered by 11146 inward-looking 50 cm photomultiplier tubes, and an outer volume serving as entering particle shield and veto with 1885 outward-looking 20 cm phototubes. The fiducial mass of the inner volume (2 m away from the walls) is 22.5 kton.

2. Atmospheric Neutrinos with Super-K

High energy neutrinos produced in the atmosphere are detected via their interactions with nuclei in the water. The easiest ν interaction to tag and study in a water Cherenkov detector is the charged current (CC) quasi-elastic interaction:

$$\nu_l + N \rightarrow l + N', \quad (2)$$

where the flavor l of the outgoing lepton tags the flavor of the incoming neutrino. The flavor of this lepton is determined using the Cherenkov ring: events are identified as “ μ -like” (non-showering) or “ e -like” (showering) based on a likelihood analysis of the Cherenkov light around the cone. At higher energies (more than a few GeV), more complicated single and multi-pion products from both charged current and neutral current (NC) neutrino interactions with nuclei predominate.

Atmospheric neutrinos are divided into three classes for Super-K:

1. **Fully-contained events (FC):** events for which the products of the neutrino interaction are completely contained within the inner detector volume. These are further subdivided into “sub-GeV” (with visible energy <1.33 GeV) and “multi-GeV” (>1.33 GeV) events. For the current analysis, single ring (mostly quasi-elastic charged current) interactions are selected. According to Monte Carlo (MC), the FC e -like sample contains about 86% CC ν_e , 4% CC ν_μ and 10% NC interactions; the FC μ -like sample contains about 96% CC ν_μ , 4% CC ν_e and $<1\%$ NC interactions.
2. **Partially-contained events (PC):** events for which the produced muon exits the inner detector volume (only muons are penetrating enough). Such events comprise a 98% pure sample of ν_μ CC interactions, according to MC. There is no single ring selection for partially contained events. The average energy of a neutrino producing a PC event in Super-K is about 15 GeV.
3. **Upward-going muons:** upward-going muons result from neutrinos which interact in the rock below the detector to produce a penetrating muon. As for PC

events, we assume the neutrino parent flavor is ν_μ , since only muon flavor neutrinos can produce penetrating leptons. These muons may either traverse the entire detector or stop inside the volume. Through-going upward muons have average parent neutrino energies of about 100 GeV; stopping upward muons have average parent neutrino energies of about 10 GeV. (Of course, there are also downward-going neutrino-induced muons, but we cannot distinguish these from the large background of entering downward-going cosmic ray muons).

Details of the event selection and reconstruction (energy, vertex position, direction, and number of rings), and of the MC are described elsewhere ^{4,5,6,7}.

3. Recent Results

3.1. What's New

The new preliminary data sample, approved in December 1998, is described in Table 1.

Table 1. Summary of June 1998 and December 1998 data and MC samples.

| DATA | | |
|----------------------------|---------------------|--------------------------|
| | June 1998 | December 1998 |
| Analyzed ivetime: | | |
| Fully-contained | 535 days | 736 days |
| Partially-contained | 535 days | 685 days |
| Upward-going muons | 516 days | 516 days |
| MONTE CARLO | | |
| | June 1998 | December 1998 |
| Generated livetime | 10 years | 20 years |
| High energy cross-sections | CCFR | GRV94 PDF ⁽⁸⁾ |
| Solar epoch | solar cycle average | solar cycle minimum |

This new sample incorporates additional livetime for FC and PC events. There were some minor improvements in reconstruction (fitting, ring counting, etc.). The MC, however, is a completely new sample. The most important differences are indicated in the table. The net effect of the change is an increase in the number and the fraction of multi-ring events at higher energies. Twenty years of livetime were

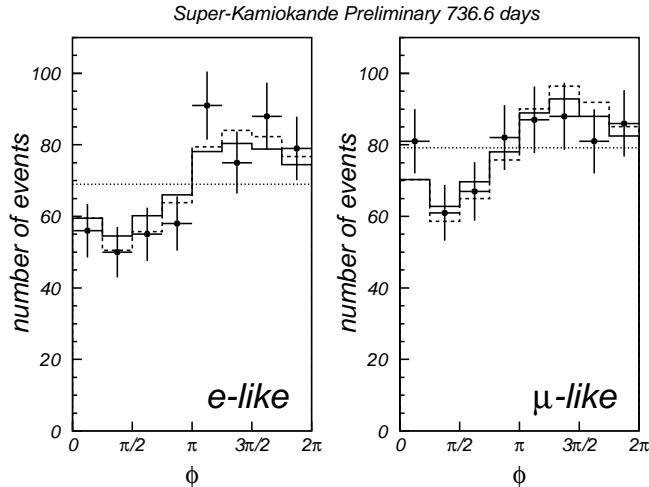


Fig. 1. The east-west effect: azimuthal distribution for low-energy near-horizon e -like and μ -like data, along with MC predictions based on Honda (solid line) and Bartol (dashed line) fluxes. $\phi = 0$ corresponds to particles going to the north and $\phi = \pi$ corresponds to particles going to the south. The expected deficit of neutrinos from the east due to the geomagnetic cutoff of the charged primaries is observed.

generated (previously there had been only 10 years).

3.2. Fully and Partially-contained events

3.2.1. East-West Effect

The east-west effect results from the action of the geomagnetic field on the charged cosmic ray primary particles. Protons at the horizon with energies less than about 50 GeV/c coming from the east are suppressed relative to those coming from other directions, where the momentum cutoff is smaller (~ 10 GeV/c). To check the reliability of both our experimental results and the atmospheric neutrino flux calculations, we have selected a sample of neutrinos for which the east-west effect is expected to be important: for which $|\cos \theta| < 0.5$ and momentum is between 400 and 3000 MeV/c.

Figure 1 shows the azimuthal distribution for both e -like and μ -like events, along with two flux predictions^{2,9}). The expected deficit from the east is observed. This analysis has been described in detail elsewhere¹⁰).

3.2.2. Ratio of Ratios

The measured flavor ratio is conventionally compared to expectation as the “ratio

of ratios”, R , defined as

$$R = \frac{(N_\mu/N_e)_{DATA}}{(N_\mu/N_e)_{MC}}, \quad (3)$$

where N_μ and N_e are numbers of μ -like and e -like events for data and MC. These numbers (Honda flux²) are given in Table 2, and the new values of R are

$$R_{FC} = 0.67 \pm 0.02(\text{stat}) \pm 0.05(\text{sys}) \quad (4)$$

for sub-GeV FC events, and

$$R_{FC+PC} = 0.66 \pm 0.04(\text{stat}) \pm 0.08(\text{sys}) \quad (5)$$

for multi-GeV FC and PC events. If there are no neutrino oscillations, R is expected to be 1. However, R is significantly smaller than 1 for both sub-GeV and multi-GeV data. A significantly low value of R has been measured by several experiments in the past^{11,12}), and recently by the Soudan collaboration with an iron-calorimeter detector¹³).

Table 2. Numbers of events for FC and PC data and Monte Carlo.

| SUB-GEV | | | MULTI-GEV | | |
|---------------|------|--------|-------------------|------|--------|
| | Data | MC | | Data | MC |
| Single ring: | | | Single ring: | | |
| e -like | 1607 | 1510.5 | e -like | 386 | 357.4 |
| μ -like | 1617 | 2277.8 | μ -like | 301 | 415.9 |
| Multiple ring | 1271 | 1614.3 | Multiple ring | 737 | 925.7 |
| Total | 4495 | 5402.5 | Total | 1424 | 1698.9 |
| | | | PC (μ -like) | 374 | 528.7 |

3.2.3. Angular Distributions

To study the pathlength dependence of the disappearance of atmospheric muon neutrinos, we can study the flux as a function of zenith angle: the Cherenkov ring direction is correlated with the neutrino direction. Angular distributions for FC and PC events are shown in Figure 2; $\cos \theta = -1$ corresponds to upward-going neutrinos and $\cos \theta = +1$ corresponds to downward-going. The oscillation prediction for the best fit parameters (see the next section) for $\nu_\mu \rightarrow \nu_\tau$ oscillation is superimposed.

For multi-GeV events, Figure 3 shows the angular distributions in 10 bins, showing that the oscillation prediction matches the data through the rapidly changing region near the horizon.

The zenith angle asymmetry A , defined as $A = \frac{U-D}{U+D}$, is shown as a function of momentum for e -like and μ -like events. The value of the asymmetry for multi-GeV

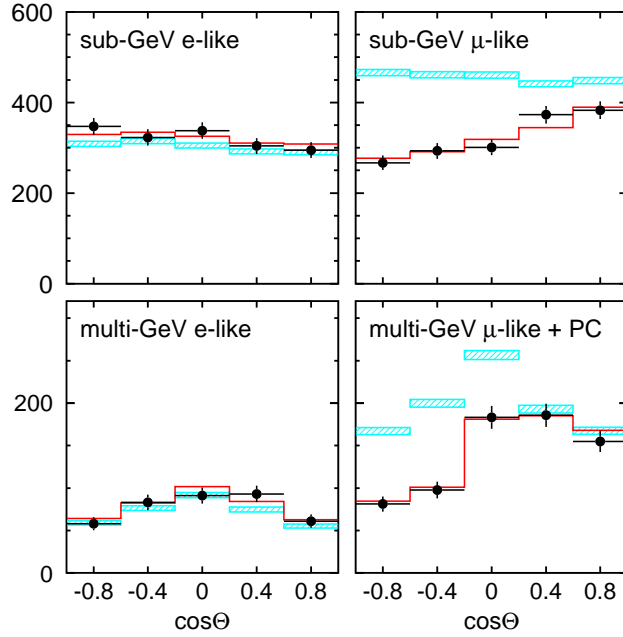


Fig. 2. Angular distributions for e -like (left) and μ -like (right) events, for sub-GeV (top) and multi-GeV (bottom) samples. The bars show the MC no-oscillation prediction with statistical errors, and the line shows the oscillation prediction for the best-fit parameters, $\sin^2 2\theta = 1.0$ and $\Delta m^2 = 3.5 \times 10^{-3} \text{ eV}^2$.

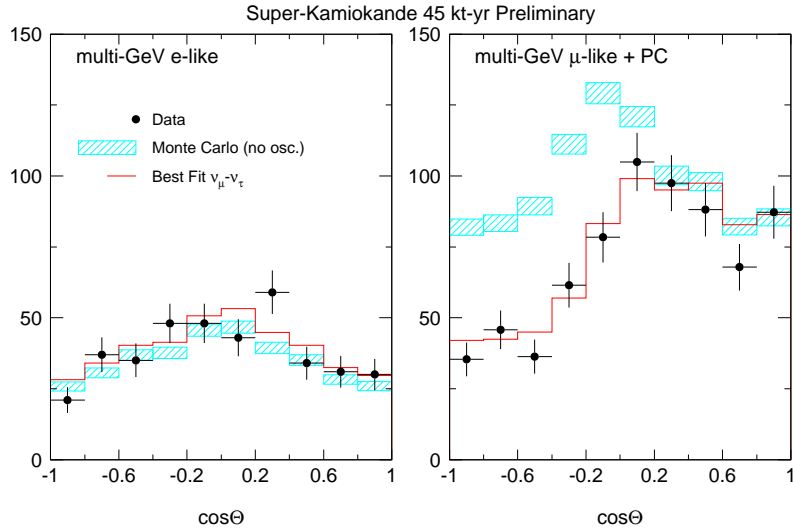


Fig. 3. Angular distributions for e -like (left) and μ -like (right) multi-GeV events (FC+PC), divided into 10 angular bins.

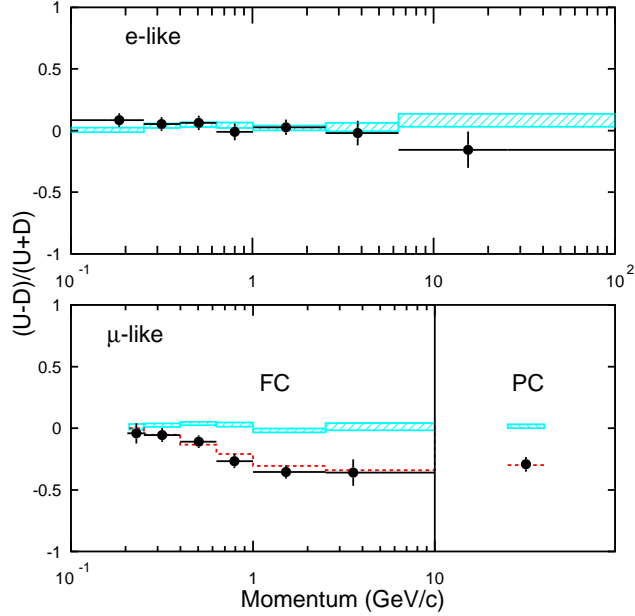


Fig. 4. Asymmetry as a function of momentum for e -like and μ -like events. For PC events the average neutrino energy is 15 GeV (the produced lepton exits and does not deposit all of its energy). The dashed line shows the oscillation prediction for the best-fit parameters.

events (including PC) is $A_{data} = -0.31 \pm 0.04$, more than 7σ from the expected value of zero, $A_{MC} = 0.01 \pm 0.01$.

3.2.4. Oscillation Fit

The oscillation fit is performed by constructing a χ^2 quantity,

$$\chi^2 = \sum_{p, \cos\theta, e, \mu} \frac{(N_{data} - N_{osc})^2}{\sigma^2} + \sum_j \frac{\epsilon_j^2}{\sigma_j^2}. \quad (6)$$

The sum is over five bins in $\cos\theta$, seven bins in $\log p$, where p is momentum, and two particle ID bins (e and μ). N_{data} is the number of data events in the bin, σ is the statistical error on data and MC, and N_{osc} is a weighted sum over events:

$$N_{osc} = \frac{\mathcal{L}_{data}}{\mathcal{L}_{MC}} \sum_{\text{events}} w(\sin^2 2\theta, \Delta m^2, \alpha, \epsilon_j), \quad (7)$$

where α is the flux normalization, $\sin^2 2\theta$ and Δm^2 are the oscillation parameters, and \mathcal{L}_{data} and \mathcal{L}_{MC} are the data and MC livetimes. The ϵ_j values and their corresponding σ_j 's take into account systematic uncertainties. Table 3 lists these systematic parameters, their estimated sigmas and their best-fit values.

To build an allowed region:

Table 3. Estimated systematic parameters. Note that the flux normalization α is not constrained in the fit.

| Systematic parameter | Estimated σ | Value at best-fit |
|--|--------------------|-------------------|
| Flux normalization, α | ($\sim 25\%$) | 8.4% |
| Energy spectrum power law, $E^{2.7\pm\delta}$ | 0.05 | -0.004 |
| μ -like/ e -like ratio, sub-GeV, β_s | 8% | 1.5% |
| μ -like/ e -like ratio, multi-GeV, β_m | 12% | -12.5% |
| FC/PC ratio, ρ | 8% | -2.9% |
| Zenith angle asymmetry, sub-GeV, η_s | 2.4% | -0.4% |
| Zenith angle asymmetry, multi-GeV, η_m | 2.7% | -0.2% |
| $\langle L/E_\nu \rangle$, λ | 15% | -1.1% |

- This χ^2 quantity is minimized at each $\sin^2 2\theta$, Δm^2 value, with respect to the systematic parameters ϵ_j .
- The minimum χ^2 in $\sin^2 2\theta$, Δm^2 parameter space, χ_{min}^2 is found.
- A confidence level map is built as a function of $\chi^2 - \chi_{min}^2$. The unphysical region is taken into account according to a two-dimensional generalization of the Particle Data Book prescription^{14,7)}.

Figure 5 shows the allowed regions for 68%, 90% and 99% C.L. for $\nu_\mu \rightarrow \nu_\tau$ oscillation. For this case, 90% C.L. corresponds to $\chi_{min}^2 + 5.3$. The best-fit oscillation parameter values in the physical region are $\sin^2 2\theta = 1.0$ and $\Delta m^2 = 3.5 \times 10^{-3} \text{ eV}^2$, corresponding to $\chi^2/d.o.f. = 62/67$. Figure 6 shows the distribution of residuals for the 70 terms in the χ^2 sum at χ_{min}^2 ; it is well fit by a normalized Gaussian. All of the best-fit ϵ_j values lie within their estimated uncertainties at the 1σ level. The $\chi^2/d.o.f.$ value for the no-oscillation hypothesis is 175/69, corresponding to a probability of less than 0.0001%.

Figure 7 shows the new allowed region compared with the June 1998 region and the old Kamiokande result¹¹⁾.

3.3. Upward-going Muons

We can get neutrino oscillation information from the upward-going muon (upmu) sample by comparing the angular distribution to the expected one. In addition, although we can get no direct energy information, we do know that the stopping and through-going samples come from different parent neutrino energy distributions, so that the stopping to through-going ratio is a way of testing the energy dependence of the oscillation hypothesis.

The through-going upward muon angular distribution is shown in Figure 8. The overall stop/through ratio is given by $\frac{N_{stop}}{N_{thru}} = 0.22 \pm 0.03$, compared to the expected

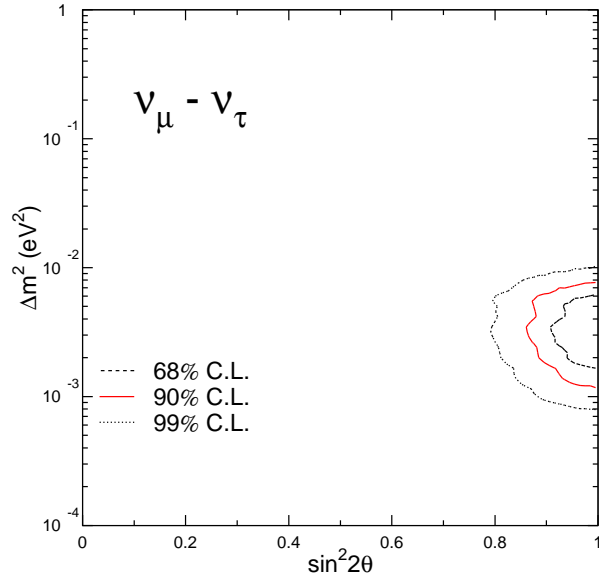


Fig. 5. Allowed regions for $\nu_\mu \rightarrow \nu_\tau$ oscillations, for FC and PC data.

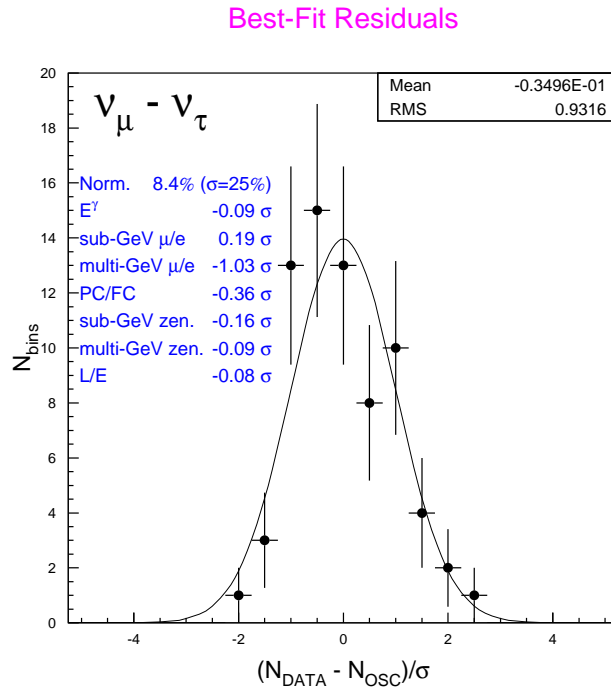


Fig. 6. Fit residuals: distribution of χ^2 residuals for the 70 bins in the equation 6 sum at χ^2_{min} . The table on the left indicates the ϵ_j best-fit values.

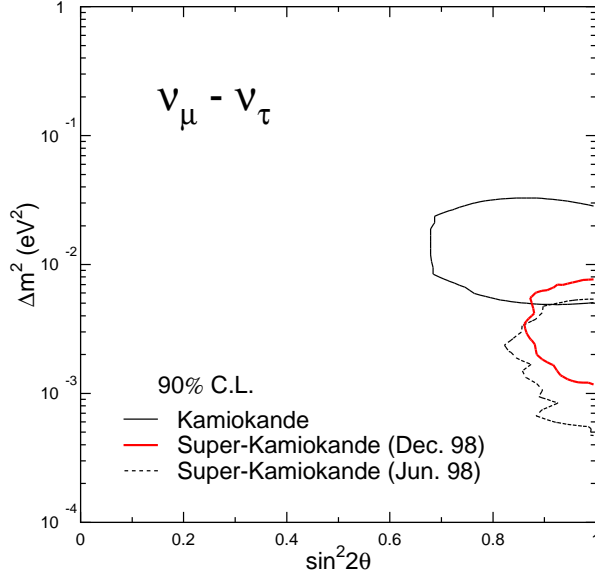


Fig. 7. 90 % C.L. allowed regions compared with the June 1998 Super-K result and the Kamiokande result.

value (using the Honda flux²⁾) of $\frac{N_{stop}}{N_{thru}} = 0.37 \pm 0.04$ for the no-oscillation case. The stop/through ratio as a function of angle is shown in Figure 8.

The oscillation fit is done by construction of a χ^2 similar to equation 6:

$$\chi^2 = \sum_{i=1}^{15} \frac{(\Phi_{data} - \Phi_{osc})^2}{\sigma^2} + \left(\frac{\alpha}{\sigma_\alpha}\right)^2 + \left(\frac{\eta}{\sigma_\eta}\right)^2, \quad (8)$$

where the sum is over 10 zenith angle bins for through-going muons and five zenith angle bins for stopping muons. For this case, the weighted MC prediction is replaced by a flux calculation²⁾, and

$$\Phi_{osc} = \Phi_{calc}(\sin^2 2\theta, \Delta m^2) * (1 + \alpha) \quad \text{for through-going muons, and} \quad (9)$$

$$\Phi_{osc} = \Phi_{calc}(\sin^2 2\theta, \Delta m^2) * (1 + \alpha)(1 + \eta) \quad \text{for stopping muons.} \quad (10)$$

α is the absolute flux normalization ($\sigma_\alpha \sim 22\%$) and η corresponds to the relative stopping and through-going uncertainty ($\sigma_\eta \sim 13\%$). The 90% C.L. allowed region (including both through-going and stopping upmu information) is shown in Figure 9. The best-fit oscillation parameters are $\sin^2 2\theta = 1$ and $\Delta m^2 = 3.2 \times 10^{-3} \text{ eV}^2$, corresponding to $\chi^2/d.o.f. = 8/13$.

3.4. Combined Analysis

We can combine FC/PC and upmu data¹⁵⁾ for a global fit by constructing a

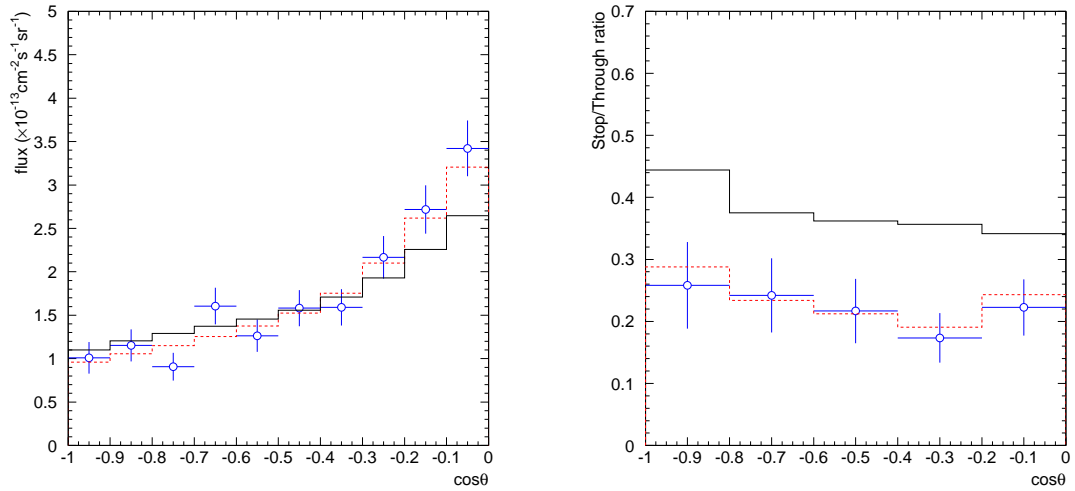


Fig. 8. Left: Angular distribution of through-going upward muons. The circles represent the data, the solid line represents the normalized no-oscillation flux prediction, and the dashed line represents the best fit prediction for oscillations. Right: ratio of stopping to through-going muons as a function of $\cos\theta$.

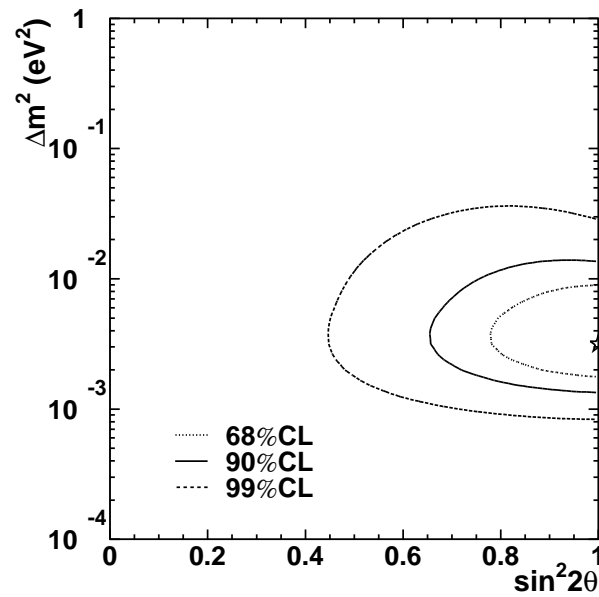


Fig. 9. $\nu_\mu \rightarrow \nu_\tau$ allowed regions for upward-going muons.

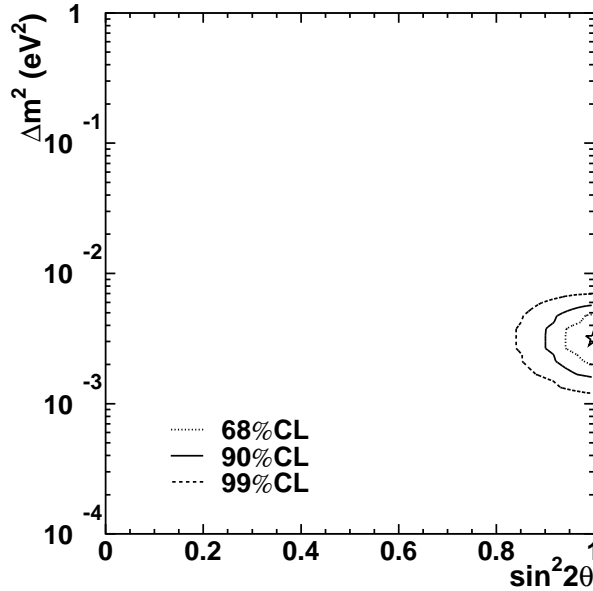


Fig. 10. Allowed regions using combined information from FC, PC and upward-going muons.

χ^2 quantity including information from both the FC/PC and upmu χ^2 quantities (equations 6 and 8):

$$\chi^2 = \sum \frac{(N_{data} - N_{osc})^2}{\sigma^2} + \sum_j \frac{\epsilon_j^2}{\sigma_j^2}, \quad (11)$$

where the sum is over the 70 FC/PC bins, and the 15 upmu bins. For FC/PC bins, N_{osc} represents the weighted MC term of the FC/PC fit, whereas for the upmu bins, N_{osc} represents the flux prediction. The systematic parameters ϵ_j include the same FC/PC terms as before; there is a common flux normalization parameter α (unconstrained, as for the FC/PC fit) and a common spectral index uncertainty δ . In addition the parameter η of the upmu fit is replaced by two parameters η_1 and η_2 , each with an assigned σ of 7%, representing the relative stopping and through-going uncertainty and the relative FC/PC and upmu uncertainty respectively.

The resulting $\nu_\mu \rightarrow \nu_\tau$ confidence level contours are shown in Figure 10. The best-fit value is at $\sin^2 2\theta = 1$ and $\Delta m^2 = 3.2 \times 10^{-3} \text{ eV}^2$, corresponding to $\chi^2/d.o.f.$ of 70.2/82.

3.5. FC Multiple Rings

An additional FC sample can be used to check for consistency of oscillation behavior: the multiple ring component of the FC sample (all FC results so far have been for

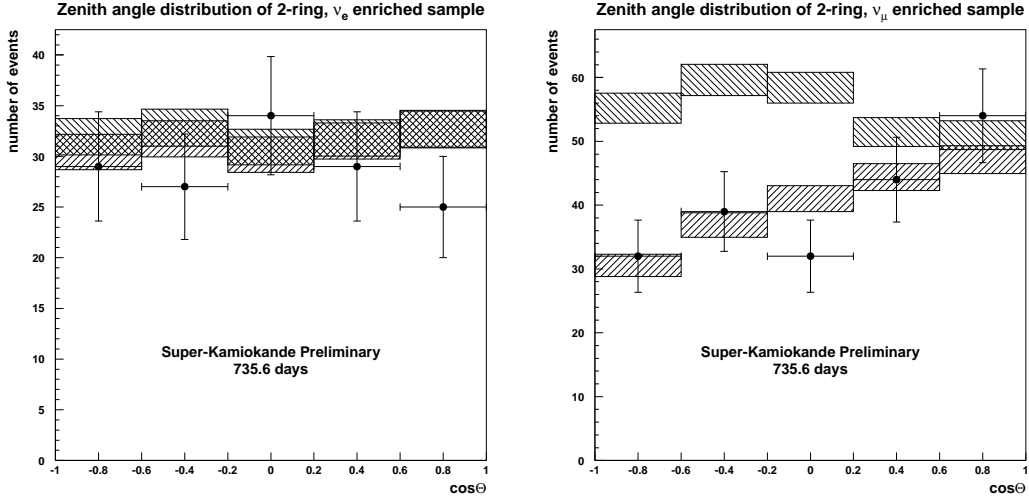


Fig. 11. Left: angular distribution for ν_e enriched sample of multiple-ring events. The left-hatched bars show the MC prediction for no oscillation and the right-hatched bars show the prediction for the oscillation parameters $\sin^2 2\theta = 1$ and $\Delta m^2 = 3.5 \times 10^{-3} \text{ eV}^2$. Right: ν_μ -enriched sample.

single rings, to tag the simplest quasielastic interactions). To produce enriched muon and electron flavor 2-ring samples, sub-GeV 2-ring events were required to satisfy the following conditions:

- $p > 300 \text{ MeV}$.
- For ν_e -enriched: 2 e -like rings not in the π^0 peak (see Section 4.2.2) or 1 e -like ring and 1 μ -like ring with the e -like ring having higher momentum. For either case, there must be no muon decay electrons.
- For ν_μ -enriched: 2 μ -like rings or 1 e -like ring and 1 μ -like ring with the μ -like ring having higher momentum. For either case, there must be at least one muon decay electron.

According to MC, the enriched ν_e sample is 60% ν_e CC, 8% ν_μ CC and 32% NC, and the enriched ν_μ sample is 89% ν_μ CC, 2% ν_e CC and 8% NC. The angular distributions for this preliminary analysis are shown in Figure 11. Clearly, the results are consistent with the oscillation hypothesis.

4. Oscillation Interpretation

For all of the allowed regions so far, we have been assuming that the muon disappearance results from ν_μ to ν_τ oscillation. However, this assumption is not necessarily

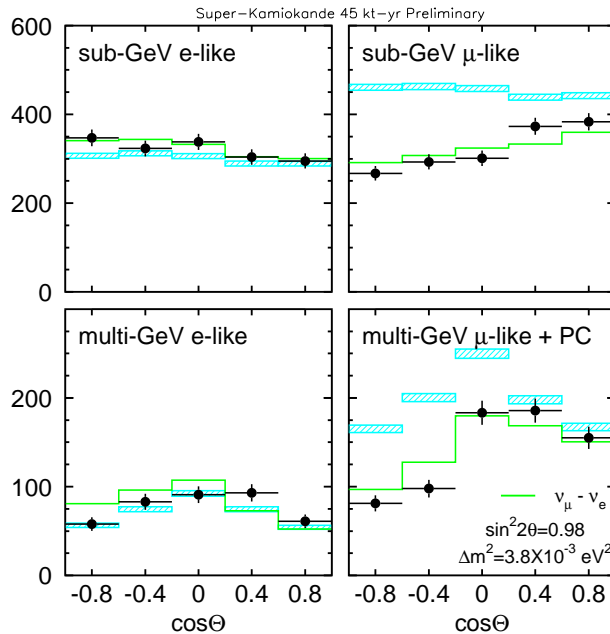


Fig. 12. Angular distributions with the best fit for $\nu_\mu \rightarrow \nu_e$ superimposed.

true. What can we say about the flavors involved in the oscillation?

4.1. $\nu_\mu \rightarrow \nu_e$

Are the muon neutrinos oscillating into electron neutrinos? This is a fairly easy question to answer – the Super-K angular distribution by itself is inconsistent with pure $\nu_\mu \rightarrow \nu_e$ oscillation. This assumption (including matter effects in the Earth) yields a very poor fit: $\chi^2/d.o.f. = 110/67$ (see Figure 12). In addition, the CHOOZ experiment in France rules out this hypothesis (for $\bar{\nu}_e$ disappearance)¹⁶.

4.2. $\nu_\mu \rightarrow \nu_s$

Could the muon neutrinos be oscillating into a non-weakly interacting sterile neutrino? With Super-K data alone, it is hard to tell this hypothesis apart from the $\nu_\mu \rightarrow \nu_\tau$ hypothesis; we expect only tens of CC ν_τ interactions in the current sample, and the products of such interactions in our detector are nearly indistinguishable from other atmospheric neutrino events. However, an oscillation to a sterile neutrino could nevertheless leave subtle imprints on some properties of our data set. Here two preliminary studies are described.

4.2.1. Angular Distribution

Due to the fact that sterile neutrinos do not exchange Z bosons with nucleons in

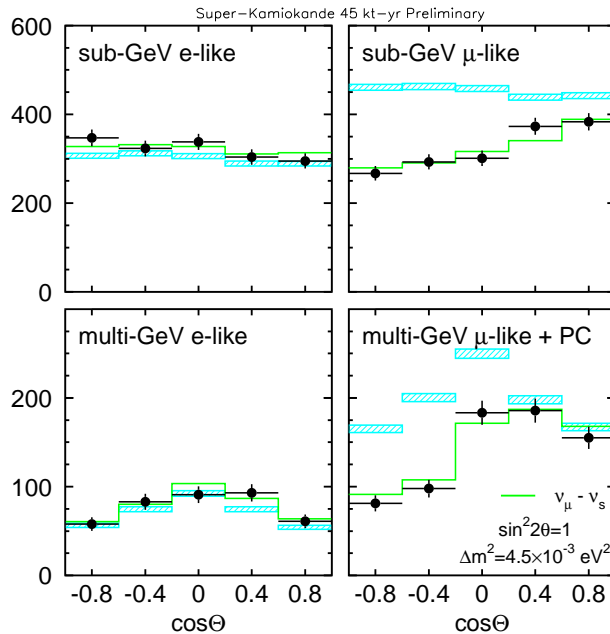


Fig. 13. Angular distributions with the best fit for $\nu_\mu \rightarrow \nu_s$ superimposed.

the earth, the angular distribution for $\nu_\mu \rightarrow \nu_s$ will be distorted with respect to the $\nu_\mu \rightarrow \nu_\tau$ oscillation case (see, for instance, Lipari and Lusignoli ¹⁷). This effect is expected to be largest for high E and low Δm^2 cases. The effect is, however, smeared over a distribution of neutrino energies.

Figure 13 shows the fit for $\nu_\mu \rightarrow \nu_s$: a good fit ($\chi^2/d.o.f. = 64/67$) is obtained. The corresponding allowed region is shown in Figure 14; it is slightly smaller than the corresponding $\nu_\mu \rightarrow \nu_\tau$ region, due to additional constraints from the matter effect in the earth. We have not yet included the high energy upward muon sample in this analysis.

4.2.2. Single Neutral Pions

A rather promising way to distinguish the tau and sterile oscillation cases is via NC neutrino interactions in the detector which produce single neutral pions. Sterile neutrinos have no NC interactions; therefore, fewer π^0 events than expected for the $\nu_\mu \rightarrow \nu_\tau$ case would be a signature of oscillation to a sterile neutrino.

The signature of a π^0 NC event in the detector is a pair of e -like rings (γ -induced electromagnetic showers) from the decay of the pion, $\pi^0 \rightarrow \gamma\gamma$. We can select a sample of such events by selecting events with exactly two e -like rings and no muon decay electrons. Figure 15 shows the reconstructed invariant mass distribution of this selected sample. The π^0 peak is clearly visible. We further reduce and enrich the sample by making an invariant mass cut of $90 \text{ MeV}/c^2 < M_{\gamma\gamma} < 190 \text{ MeV}/c^2$. According to MC, the events surviving this cut are an 84% pure sample of NC interactions. The

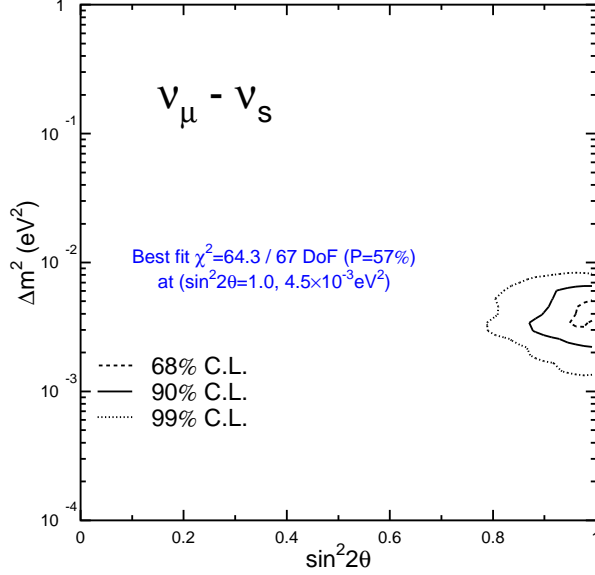


Fig. 14. Allowed region for $\nu_\mu \rightarrow \nu_s$.

angular distribution of these events is shown in Figure 15.

We can also take the ratio of π^0/e -like events and compare it to the expected value for MC. The FC single ring e -like sample is mostly CC interactions of non-oscillated ν_e 's. This ratio of ratios should be nearly 1 if muon neutrinos are oscillating to tau neutrinos (because tau neutrinos interact via NC), and less than 1 if muon neutrinos are oscillating into sterile neutrinos. Table 4 shows the numbers.

Table 4. π^0 candidates.

| | Data | MC |
|--------------------------------------|-------|-------|
| π^0 -like | 279 | 253.6 |
| π^0 -like, background-subtracted | 231.8 | 195.9 |

The result is:

$$\frac{(\pi^0/e)_{DATA}}{(\pi^0/e)_{MC}} = 1.03 \pm 0.06(\text{data stat}) \pm 0.02(\text{MC stat}) \pm 0.24(\text{sys}) \quad (12)$$

If the background is subtracted, the result is:

$$\frac{(\pi^0/e)_{DATA}}{(\pi^0/e)_{MC}} = 1.11 \pm 0.06(\text{data stat}) \pm 0.02(\text{MC stat}) \pm 0.26(\text{sys}) \quad (13)$$

Notice that the systematic contribution to the uncertainty exceeds the statistical contribution by a large factor. The systematic uncertainty is in fact dominated

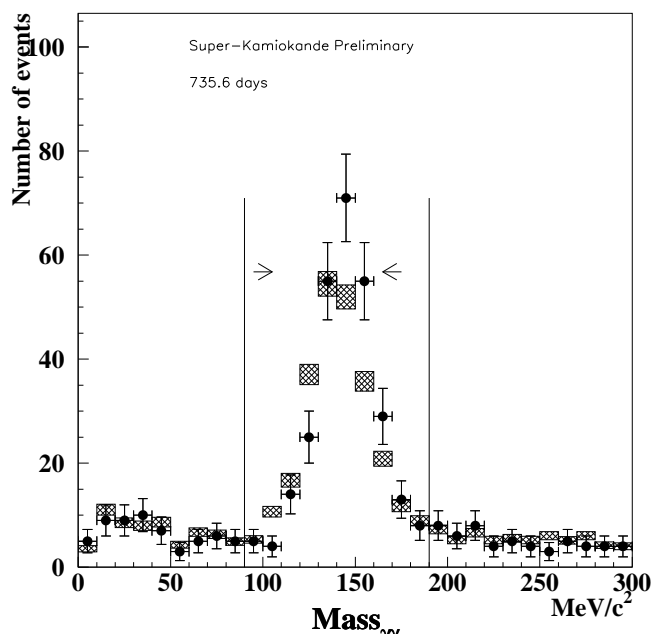


Fig. 15. Invariant mass distribution for π^0 -like events selected according to the criteria given in the text. The mass cut is shown.

by uncertainties in the π^0 production cross-section in water. The K2K collaboration¹⁸⁾ hopes to reduce this uncertainty by high statistics measurements of neutrino interactions in its near water detector.

5. Summary

Table 5 summarizes the status of fits of the new Super-K data to three possible two-flavor oscillation scenarios. We obtain good fits for $\nu_\mu \rightarrow \nu_\tau$ and $\nu_\mu \rightarrow \nu_s$; pure two-flavor $\nu_\mu \rightarrow \nu_e$ is ruled out. More work is currently in progress.

6. Acknowledgements

The Super-Kamiokande experiment is supported by the Japanese Ministry of Education, Science, Sports and Culture and the United States Department of Energy.

7. References

- 1) Y. Fukuda *et al.*, *Phys. Rev. Lett.* **81** (1998) 1562. hep-ex/9807003
- 2) M. Honda *et al.*, *Phys. Rev.* **D52** (1995) 4985, *Prog. Theor. Phys. Suppl.* **123** (1996) 483.
- 3) G. Barr *et al.*, *Phys. Rev.* **D39** (1989) 3532. V. Agrawal *et al.* *Phys. Rev.*

Table 5. Summary of two-flavor oscillation fits for new Super-K results.

| No-oscillation fits | | | |
|----------------------------|--|--|-----------------|
| | | | $\chi^2/d.o.f.$ |
| FC/PC | | | 175/69 |
| upmu | | | 41/15 |
| combined | | | 214/84 |

| Fits to $\nu_\mu \rightarrow \nu_\tau$ | | | |
|--|---------------------------------|------------------|-----------------|
| | Δm^2 (eV ²) | $\sin^2 2\theta$ | $\chi^2/d.o.f.$ |
| FC/PC | 3.5×10^{-3} | 1.0 | 62.1/67 |
| upmu | 3.2×10^{-3} | 1.0 | 8/13 |
| combined | 3.2×10^{-3} | 1.0 | 70.2/82 |

| Fit to $\nu_\mu \rightarrow \nu_s$ | | | |
|--|---------------------------------|------------------|-----------------|
| | Δm^2 (eV ²) | $\sin^2 2\theta$ | $\chi^2/d.o.f.$ |
| FC/PC | 4.5×10^{-3} | 1.0 | 64.3/67 |

| Fit to $\nu_\mu \rightarrow \nu_e$ | | | |
|--|---------------------------------|------------------|-----------------|
| | Δm^2 (eV ²) | $\sin^2 2\theta$ | $\chi^2/d.o.f.$ |
| FC/PC | 3.8×10^{-3} | 0.98 | 110/67 |

- D53** (1996) 1313. hep-ph/9509423 T. K. Gaisser and T. Stanev, Proc. 24th Int. Cosmic Ray Conf. (Rome) Vol. 1 (1995) 694.
- 4) Y. Fukuda *et al.*, *Phys. Lett.* **B433** (1998) 9. hep-ex/9803006
 - 5) Y. Fukuda *et al.*, *Phys. Lett.* **B436** (1998) 33. hep-ex/9805006
 - 6) Y. Fukuda *et al.*, *Phys. Rev. Lett.* **82** (1999) 2644. hep-ex/9812014
 - 7) M. D. Messier, PhD thesis, Boston University (1999).
 - 8) M. Gluck, E. Reya and A. Vogt, *Z. Phys.* **C67**, 433 (1995).
 - 9) P. Lipari, T. K. Gaisser and T. Stanev, *Phys. Rev.* **D 58**, (1998) 073003. hep-ph/9803440
 - 10) T. Futagami *et al.*, submitted to *Phys. Rev. Lett.*. astro-ph/9901139
 - 11) K. S. Hirata *et al.*, *Phys. Lett.* **B280** (1992) 146.
 - 12) R. Becker-Szendy *et al.*, *Phys. Rev.* **D46** (1992) 3720.
 - 13) W. W. M. Allison *et al.* *Phys. Lett.* **B449** 137 (1999). hep-ex/9901024

- 14) Particle Data Group, Review of Particle Properties, R. M. Barnett *et al.*, *Phys. Rev.* **D54**, (1996) 375.
- 15) A. Habig for the Super-Kamiokande collaboration, Proceedings of DPF '99 (UCLA). hep-ex/9903047
- 16) M. Apollonio *et al.*, *Phys. Lett.* **B420**, (1998) 397. hep-ex/9711002
- 17) P. Lipari and M. Lusignoli, *Phys. Rev.* **D58** 073005 (1998). hep-ph/9803440
- 18) Y. Oyama, talk at the YITP workshop on flavor physics, Kyoto (1998). hep-ex/9803014